THE ASTROPHYSICAL JOURNAL, 397:492–499, 1992 October 1

ON THE NATURE OF THE BIPOLAR MOLECULAR OUTFLOW IN AFGL 437

J. F. GÓMEZ,[1] J. M. TORRELLES,[2] R. ESTALELLA,[3] G. ANGLADA,[3]
L. VERDES-MONTENEGRO,[2] AND P. T. P. HO[1]
Received 1992 January 27; accepted 1992 April 7

ABSTRACT

With the IRAM 30 m telescope we have observed the CO($J = 2 \rightarrow 1$), ^{13}CO($J = 1 \rightarrow 0$), and C^{18}O($J = 1 \rightarrow 0$) rotational transition lines toward the AFGL 437 cluster. Our data show a molecular outflow with a north–south bipolarity. This bipolarity is observed in the three lines. An interesting result is that the blue and redshifted lobes are not elongated in the direction of the outflow axis, but in the east–west direction, perpendicularly to the outflow axis. Therefore, AFGL 437 appears to be an outflow with a clear bipolarity, but with a very low collimation. We propose a geometrical model in which the observed bipolar outflow is produced by a laminar flow of dragged molecular gas along the walls of a cavity or hollow, near the edge of the molecular cloud, opened by the stellar winds of the AFGL 437 cluster.

Subject headings: H II regions — ISM: individual (AFGL 437) — masers — ISM: jets and outflows

1. INTRODUCTION

The study of bipolar outflows in regions of star formation has prompted a great deal of observational and theoretical work, since they are one of the most striking phenomena related to young stars. The mechanisms proposed to explain the collimation of these bipolar outflows, such as disks or toroids (see Rodríguez 1989 for a review), implicitly assume that, at scales larger than the collimating structures, the ambient molecular gas is distributed more or less isotropically around the region of star formation.

But in a real case, the distribution of molecular gas is very likely to be far from isotropic. When energetic winds from the stars interact with the ambient molecular gas, an anisotropic distribution of this molecular gas, even far from the collimation scales, can determine the geometry of the observed outflow. How the molecular gas distribution and the outflow geometry relate to each other is then a crucial point in our understanding of the star formation processes. For this reason, we think that it is important to study regions where an anisotropic distribution of the ambient molecular gas as well as a molecular outflow are both present. This may be the case for the region AFGL 437.

AFGL 437 is a cluster of, at least, four infrared sources (Kleinmann et al. 1977; Wynn-Williams et al. 1981), two of them (AFGL 437W and AFGL 437S) coinciding with compact H II regions (Wynn-Williams et al. 1981; Torrelles et al. 1992). Its distance has been estimated to be $\sim$2 kpc (Arquilla & Goldsmith 1984, and references therein). The total luminosity of the region is $\sim 2 \times 10^4\ L_\odot$ (Parmar et al. 1987). Wynn-Williams et al. (1981) interpret their infrared and radio continuum data by suggesting that the cluster lies at the edge of the molecular cloud. Rainer & McLean (1987), on the basis of K (2.2 μm) images, suggest the presence of a strong interaction between winds associated with the stars of the cluster and the ambient gas. Water maser emission with three velocity components (-49, -39, and -28 km s^{-1}) has been detected by Gyulbudaghian, Rodríguez, & Mendoza-Torres (1987), which is an indication of mass-loss processes.

Asymmetric CO profiles were detected by Schneps et al. (1978) and interpreted as caused by rotational and radial mass motions of the molecular cloud. Afterward, when the molecular outflow phenomenon was well established in the literature (see Rodríguez et al. 1982), Arquilla & Goldsmith (1984), using CO observations with 50″ resolution and a higher sensitivity, interpreted these profiles as produced by a bipolar outflow, with the red and blue lobes located at the north and south of the central cluster, respectively, and their maxima separated by $\sim$1.′2 ($\sim$0.7 pc at 2 kpc). On the other hand, Heyer et al. (1986) found a spheroidal CS structure of size $\sim$1′, peaking at the position of the infrared cluster. These authors concluded that the detected interstellar high-density molecular structure does not play an important role in the collimation processes of the bipolar molecular outflow.

In this paper, we present observations of CO, ^{13}CO, and C^{18}O rotational transition lines carried out with the 30 m telescope of the Institut de Radio Astronomie Millimétrique (IRAM), as well as H_2O maser observations using the 37 m Haystack telescope. Our main goal with the CO, ^{13}CO, and C^{18}O observations was to study with high angular resolution the morphology and kinematics of both the bipolar molecular outflow and the ambient molecular cloud, in order to ascertain the collimation processes. Water maser observations were made to determine accurately the positions of the components detected by Gyulbudaghian et al. (1987).

2. OBSERVATIONS

2.1. *System Parameters*

The observations of the CO($J = 2 \rightarrow 1$), ^{13}CO($J = 1 \rightarrow 0$), and C^{18}O($J = 1 \rightarrow 0$) rotational transition lines were carried out in 1988 February with the IRAM 30 m telescope, at Pico Veleta (Granada, Spain). In order to do simultaneous observations of these three lines, we used two SIS receivers and two filter banks, one of 512 × 1 MHz channels (velocity resolution $\simeq$1.3 km s^{-1} at $\lambda = 1.3$ mm), and the other one of 256 × 100 kHz channels (velocity resolution $\simeq$0.3 km s^{-1} at $\lambda = 2.7$ mm)

[1] Harvard-Smithsonian Center for Astrophysics, 60 Garden Street, Cambridge, MA 02138, and Instituto de Astrofísica de Andalucía, CSIC, AP. Correos 3004, C/Sancho Panza s/n, E-18080 Granada, Spain.
[2] Instituto de Astrofísica de Andalucía, CSIC, AP. Correos 3004, C/Sancho Panza s/n, E-18089 Granada, Spain, and Harvard-Smithsonian Center for Astrophysics, 60 Garden Street, Cambridge, MA 02138.
[3] Departament d'Astronomia i Meteorologia, Universitat de Barcelona, Av. Diagonal 647, E-08028 Barcelona, Spain (postal address); and Laboratori d'Astrofísica, Societat Catalana de Física (IEC).

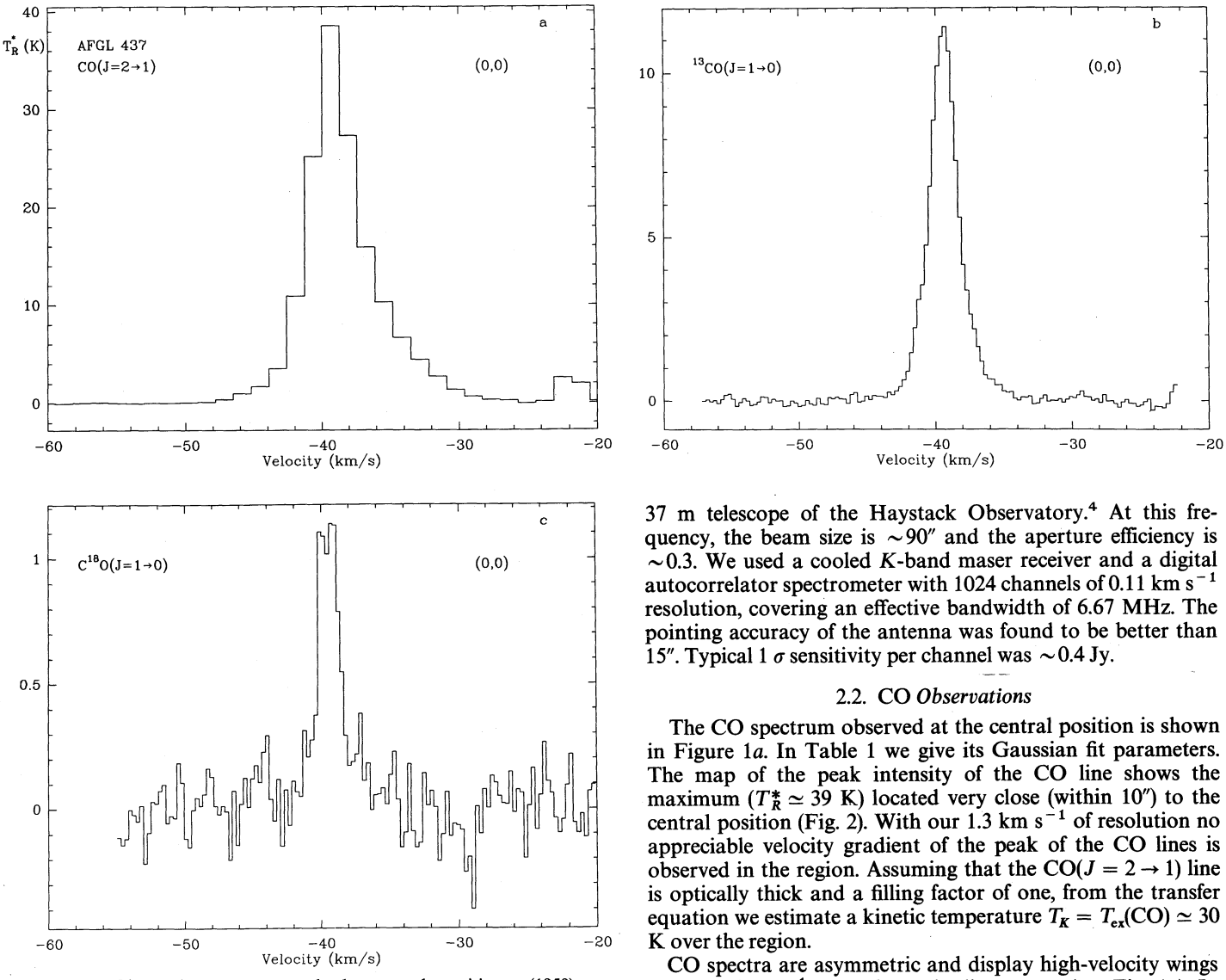

FIG. 1.—Observed spectra toward the central position, $\alpha(1950) = 03^h03^m31^s.3$, $\delta(1950) = 58°19'19''$.

split in two halves. Beam sizes (FWHM) were $\sim 13''$ ($\lambda = 1.3$ mm, CO) and $\sim 22''$ ($\lambda = 2.7$ mm, ^{13}CO and $C^{18}O$). From observations of point sources we estimate that the rms pointing error of the telescope was $\leq 3''$. Position switching mode was used. System temperatures were typically ~ 450 K. Temperatures in this paper are given in units of T_R^* (Kutner & Ulich 1981).

Our maps were centered on the position of the infrared source AFGL 437W (Wynn-Williams et al. 1981); that is, $\alpha(1950) = 03^h03^m31^s.3$ and $\delta(1950) = 58°19'19''$. Offset positions of the maps shown in this paper are given in arcseconds relative to this central position. In a few positions, the observed $C^{18}O$ spectra have not been used in our analysis due to the presence of ripples in the baselines. Typically, we obtained a 1 σ sensitivity per channel of ~ 0.05 K (CO), ~ 0.12 K (^{13}CO), and ~ 0.15 K ($C^{18}O$).

The observations of the 6_{16}–5_{23} transition of H_2O ($\nu = 22.235080$ GHz) were made in 1991 February, using the 37 m telescope of the Haystack Observatory.[4] At this frequency, the beam size is $\sim 90''$ and the aperture efficiency is ~ 0.3. We used a cooled K-band maser receiver and a digital autocorrelator spectrometer with 1024 channels of 0.11 km s^{-1} resolution, covering an effective bandwidth of 6.67 MHz. The pointing accuracy of the antenna was found to be better than $15''$. Typical 1 σ sensitivity per channel was ~ 0.4 Jy.

2.2. CO *Observations*

The CO spectrum observed at the central position is shown in Figure 1*a*. In Table 1 we give its Gaussian fit parameters. The map of the peak intensity of the CO line shows the maximum ($T_R^* \simeq 39$ K) located very close (within $10''$) to the central position (Fig. 2). With our 1.3 km s^{-1} of resolution no appreciable velocity gradient of the peak of the CO lines is observed in the region. Assuming that the CO($J = 2 \rightarrow 1$) line is optically thick and a filling factor of one, from the transfer equation we estimate a kinetic temperature $T_K = T_{ex}(CO) \simeq 30$ K over the region.

CO spectra are asymmetric and display high-velocity wings up to 15 km s^{-1} away from the line center (see Fig. 1*a*). In Figure 3 we present a contour map of the integrated intensity from $V_{LSR} = -55$ to -44 km s^{-1} (blueshifted gas) and from $V_{LSR} = -35$ to -24 km s^{-1} (redshifted gas). This map of high-velocity gas shows a bipolar morphology, which is consistent with that observed by Arquilla & Goldsmith (1984) with $50''$

[4] Radio astronomy at Haystack Observatory of the Northeast Radio Observatory Corporation (NEROC) is supported by a grant from the National Science Foundation.

TABLE 1

LINE PARAMETERS[a]

Line	T_R^* (K)	ΔV (km s^{-1})	V_{LSR} (km s^{-1})
CO($J = 2 \rightarrow 1$)	38.6 ± 0.2	3.49 ± 0.01	-39.28 ± 0.01
^{13}CO($J = 1 \rightarrow 0$)	11.4 ± 0.4	2.28 ± 0.02	-39.42 ± 0.01
$C^{18}O$($J = 1 \rightarrow 0$)	1.2 ± 0.4	1.96 ± 0.15	-39.45 ± 0.05

[a] Obtained from Gaussian fits to the observed spectra at the central position, $\alpha(1950) = 03^h03^m31^s.3$, $\delta(1950) = 58°19'19''$.

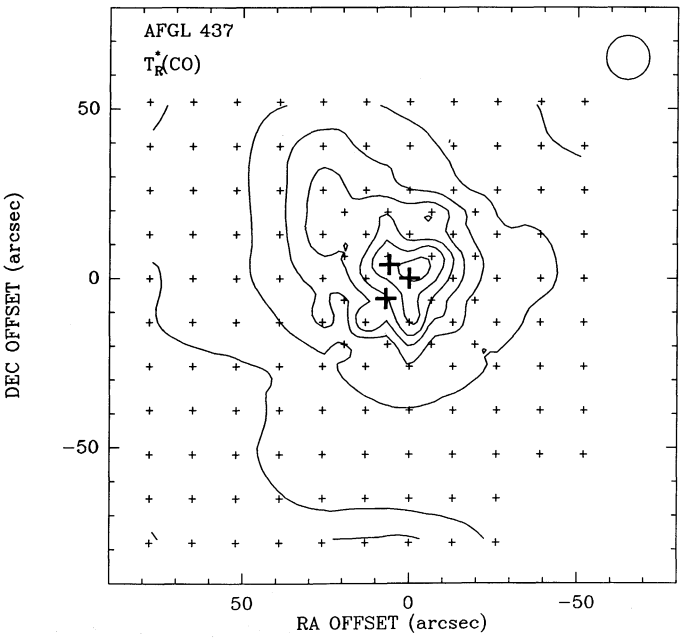

FIG. 2.—Contour map of the peak intensity of the CO($J = 2 \rightarrow 1$) line. Contour levels are 10, 14, 18, 22, 26, 30, 34, and 38 K. Small crosses indicate the observed positions. Thick crosses indicate the positions of the infrared sources AFGL 437 N, S, and W (Wynn-Williams et al. 1981). Sources AFGL 437W and AFGL 437S coincide with two compact H II regions (Wynn-Williams et al. 1981; Torrelles et al. 1992).

resolution. Our map, of higher angular resolution, reveals a more detailed structure.

The redshifted emission is located at the north of AFGL 437, while the blueshifted one is at the south, with their maxima separated by $-50''$ (~ 0.5 pc). Both lobes of blue and redshifted emission show a complex structure, with several maxima and protuberances. Interestingly, both lobes are not elongated in the direction of the outflow axis, but in the east–west direction, perpendicularly to the outflow axis. Thus, AFGL 437 is an outflow with a clear bipolarity, but with a poor degree of collimation. We also note that the AFGL 437 cluster is not located at the center of the molecular outflow.

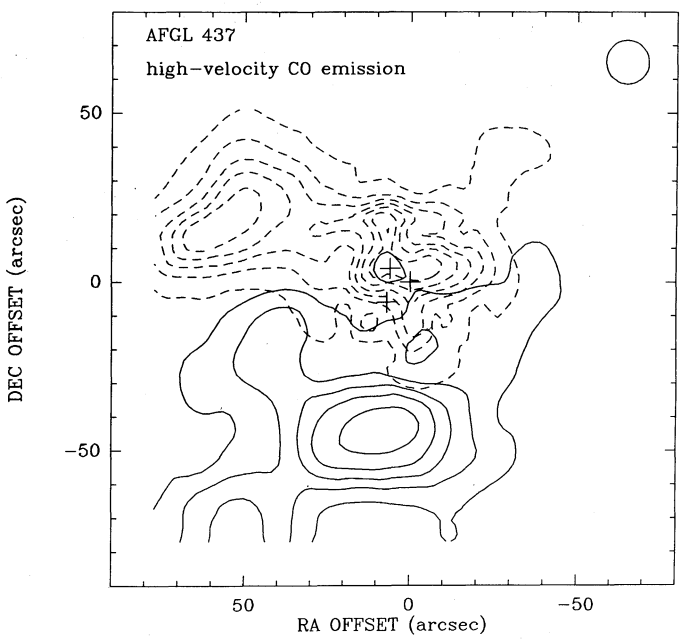

FIG. 3.—Contour map of the integrated intensity of the CO($J = 2 \rightarrow 1$) line over velocity ranges from -55 to -44 km s^{-1} (thin contours, blueshifted emission) and from -35 to -24 km s^{-1} (dashed contours, redshifted emission). Contour levels are 4, 8, 12, 16, and 20 K km s^{-1} (blueshifted emission), and 4, 8, 12, 16, 20, 24, and 28 K km s^{-1} (redshifted emission).

2.3. ^{13}CO *and* C^{18}O *Observations*

In Figures 1*b* and 1*c* we show the ^{13}CO, and C^{18}O spectra observed toward the central position. In Table 1 we give their Gaussian fit parameters. The ^{13}CO spectra show several line components over the region (Fig. 4). The velocity of these components changes along the region, and they often appear blended due to their small separation in velocity. Three of these components, centered approximately at $V_{LSR} = -43$, -39.5, and -37 km s^{-1}, are especially conspicuous. One of them corresponds to the velocity of the cloud (-39.5 km s^{-1}), while the other two are blue and redshifted lines. We note that these velocity components are not observed in the CO spectra, probably because of the lower velocity resolution and the higher opacity of the CO line.

A spheroidal structure with several maxima can be seen in the contour maps of the total integrated intensity of both ^{13}CO and C^{18}O lines (Fig. 5). From the transfer equation, assuming $T_{ex}(^{13}\mathrm{CO}) = T_{ex}(\mathrm{C}^{18}\mathrm{O}) = T_{ex}(\mathrm{CO}) = T_K \simeq 30$ K, we estimate that the opacities for the ^{13}CO and C^{18}O are $\tau_{13} \leq 1$ and $\tau_{18} \leq 0.1$ over the region. Therefore, these lines are optically thin enough to be tracing the column density of the molecular gas.

In order to find out the behavior of the velocity components, we made contour maps of the integrated intensity of the ^{13}CO lines for three velocity ranges, each of them embracing one of the components mentioned above. These velocity ranges extend from -44 to -41 km s^{-1} (blue component), -41 to -38 km s^{-1} (central component), and -38 to -35 km s^{-1} (red component). Contour maps of the integrated intensities are shown in Figure 6. An interesting result is that, as for the CO, the ^{13}CO redshifted component is mainly located in the northern areas (Fig. 6*a*), while the blueshifted component is in the southern ones (Fig. 6*c*). This suggests that the blue and redshifted components of the ^{13}CO emission are tracing the low velocity gas (inner wings) of the molecular outflow. By overlapping the half-power contours of the ^{13}CO maps (Figs. 6*a* and 6*c*) we obtain a bubble-like structure around the AFGL 437 cluster (see Fig. 6*d*).

The C^{18}O data show a behavior similar to that of the CO and ^{13}CO lines, that is, redshifted gas at the north of the region and blueshifted gas at the south.

2.4. H_2O *Maser Observations*

The main goal of the water maser observations was to determine accurately the positions of the three water maser velocity components detected in 1982 by Gyulbudaghian et al. (1987), in order to know whether they were spatially associated with the components observed in the ^{13}CO lines. In order to estimate the positions of the H_2O maser components, we made a five-point map with half-beam spacings, centered at the same reference position of the CO observations mentioned above. Our H_2O maser observations show only two components. Their estimated positions and fluxes are given in Table 2. Both positions are within 5″ from the central AFGL 437 cluster. These positions are also in good agreement (within 5″) with

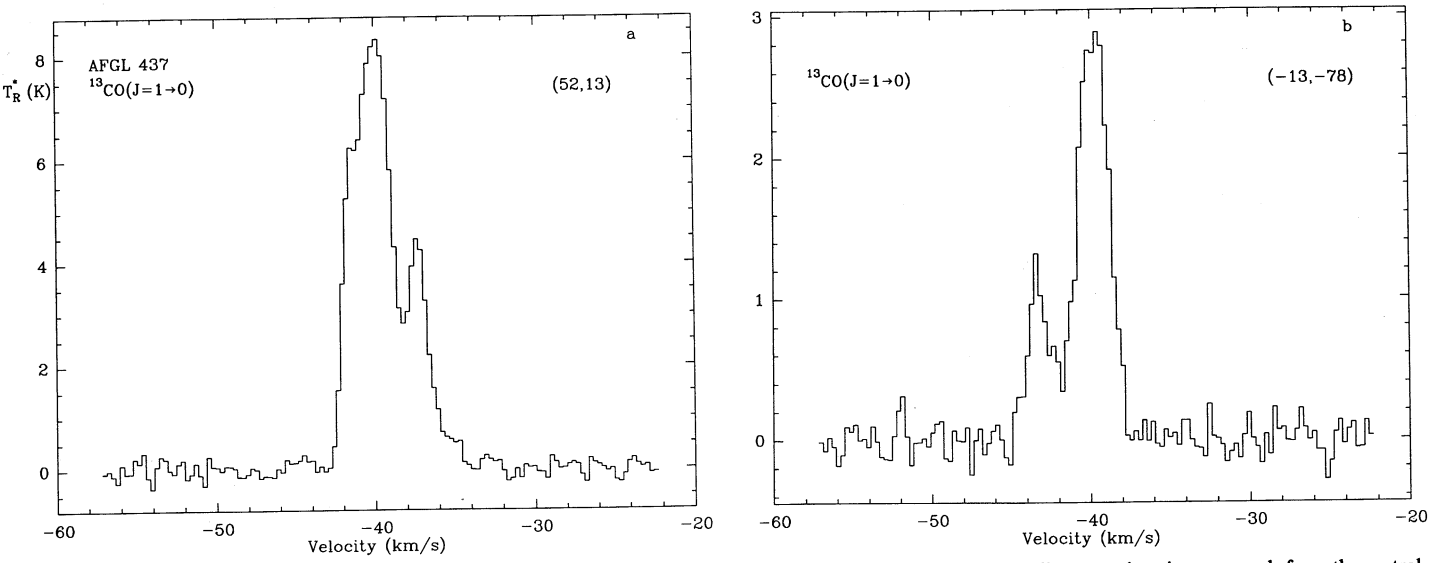

FIG. 4.—Spectra of the ^{13}CO($J = 1 \rightarrow 0$) line at two selected positions, showing several line components. Position offsets are given in arcseconds from the central position.

those obtained recently from VLA observations (Torrelles et al. 1992).

2.5. *Molecular Outflow and Ambient Cloud Parameters*

The parameters of the AFGL 437 molecular outflow and the ambient molecular cloud are given in Tables 3 and 4, respectively. To estimate the outflow parameters we have considered the integration of the ^{13}CO($J = 1 \rightarrow 0$) emission over the inner wings with velocity ranges from -44 to -41 km s^{-1} (blueshifted gas) and from -38 to -35 km s^{-1} (redshifted gas), as well as the integration of the CO($J = 2 \rightarrow 1$) emission over the outer wings (where ^{13}CO is not observable) with velocity ranges from -55 to -44 km s^{-1} (blueshifted gas) and from -35 to -24 km s^{-1} (redshifted gas). The blue and redshifted ^{13}CO components dominate the total momentum rate of the molecular outflow ($\sim 6 \times 10^{-3}$ $M_\odot$ km s^{-1} yr^{-1}), which is about one order of magnitude larger than the derived momen-

TABLE 2

H$_2$O MASER PARAMETERS

α(1950)	δ(1950)	V_{LSR} (km s^{-1})	S_ν (Jy)
03^{h}03^{m}31^s.7	58°19′22″	−25.0	9.6
03^{h}03^{m}31^s.2	58°19′23″	−37.9	4.8

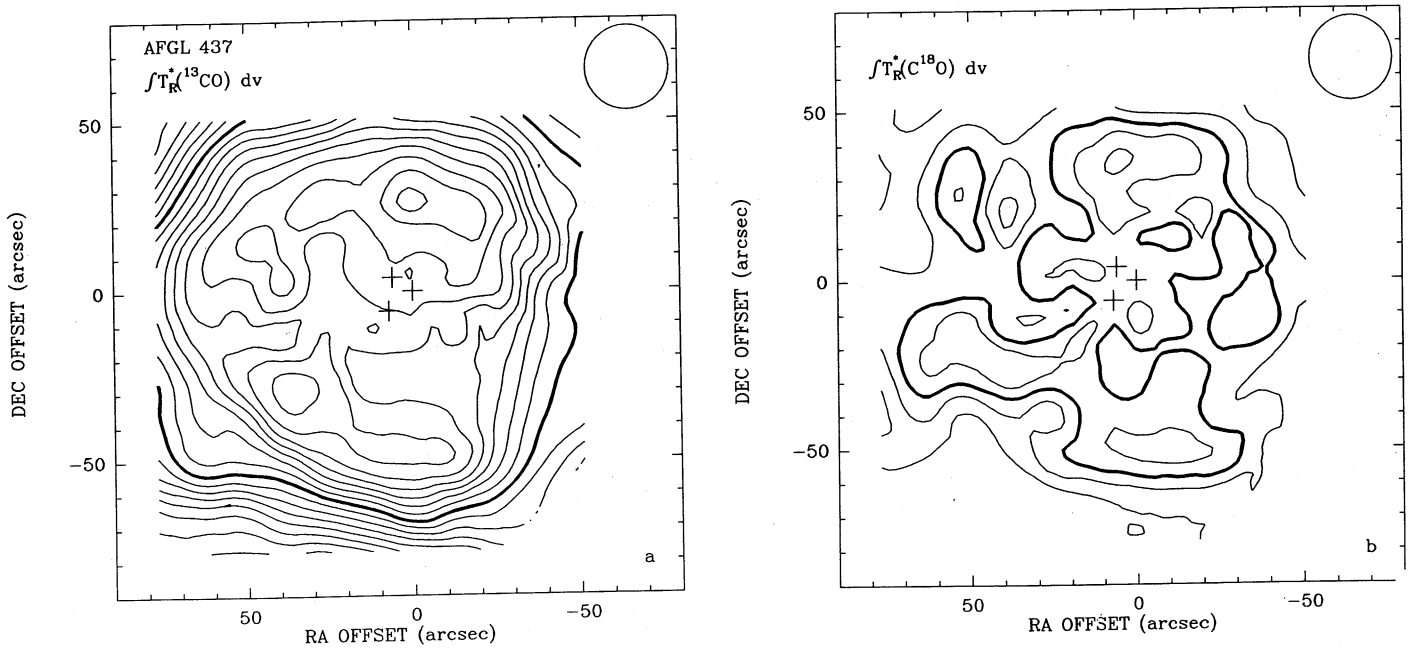

FIG. 5.—(*a*) Contour map of the integrated intensity of the ^{13}CO($J = 1 \rightarrow 0$) line, over a velocity range from -47 to -32 km s^{-1}. Contour levels range from 5 to 37 K km s^{-1} with an increment step of 2 K km s^{-1}. (*b*) Contour map of the integrated intensity of the C^{18}O($J = 1 \rightarrow 0$) line, over a velocity range from -44 to -35 km s^{-1}. Contour levels range from 0.8 to 4.8 K km s^{-1} with an increment step of 0.8 K km s^{-1}. The half-power contours are indicated with thick lines.

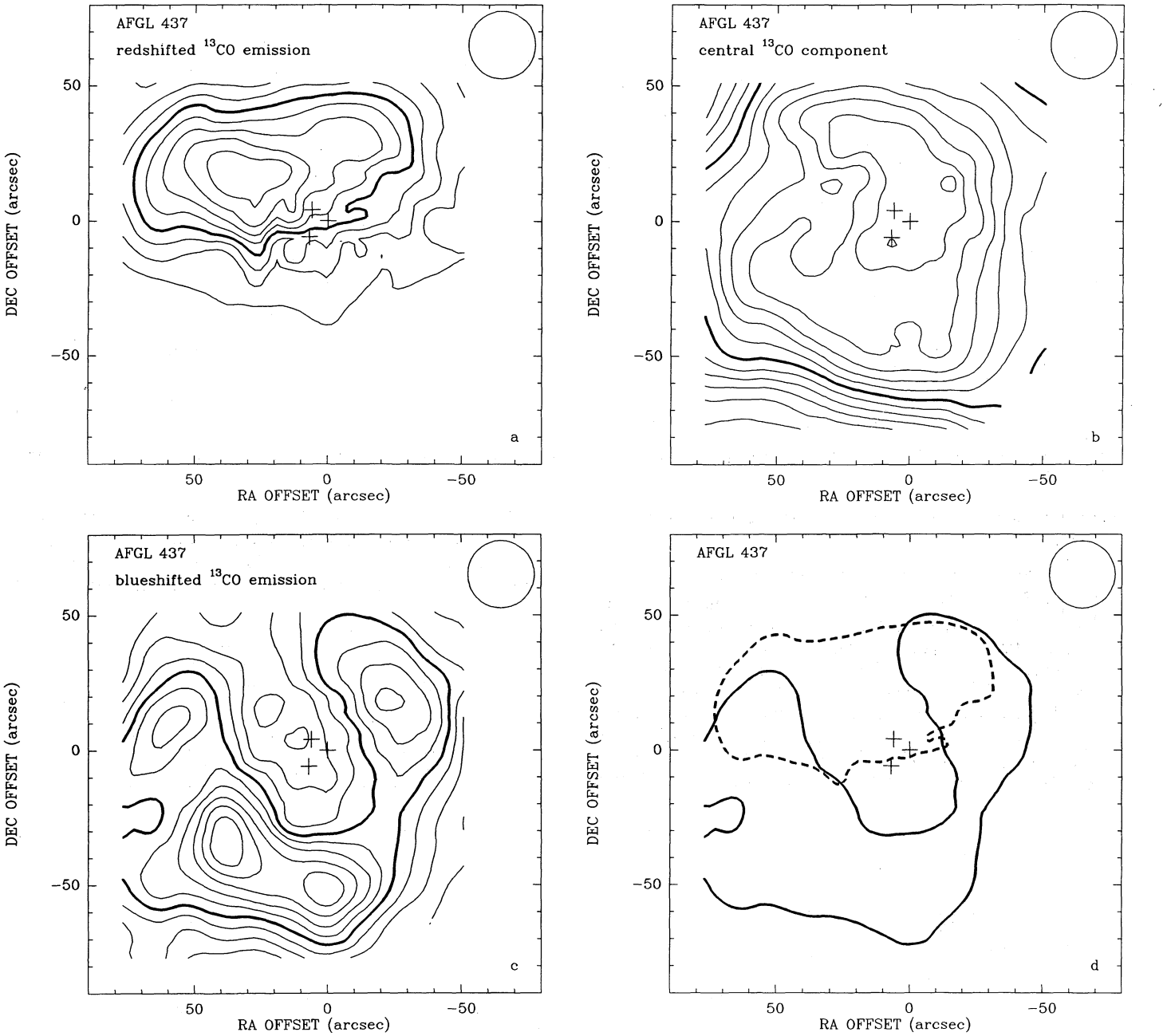

FIG. 6.—Contour maps of the integrated intensity of the ^{13}CO line over three different velocity ranges: (*a*) From -38 to -35 km s^{-1} (red component). Contour levels are 1, 2, 3, 4, 5, 6, 7, and 8 K km s^{-1}. (*b*) From -41 to -38 km s^{-1} (central component). Contour levels are 3, 5, 7, 9, 11, 13, 15, 17, 19, 21, 23, and 25 K km s^{-1}. (*c*) From -44 to -41 km s^{-1} (blue component). Contour levels are 2, 3, 4, 5, 6, 7, 8, 9, and 10 K km s^{-1}. The half-power contours of these maps are indicated with thick lines. (*d*) Overlapping of the half-power contours of the ^{13}CO red component (*a*) and blue component (*c*).

tum rate of the radiation field ($L_*/c = 4 \times 10^{-4}\ M_\odot$ km s^{-1} yr^{-1}, assuming $L_* \simeq 2 \times 10^4\ L_\odot$, Parmar et al. 1987). This difference of one order of magnitude between the values of the momentum rate of the molecular outflow and the radiation field is also observed in other molecular outflow sources (Rodríguez et al. 1982; Lada 1985), giving rise to the so-called "momentum problem" in the case where molecular outflows are driven by stellar wind momentum (see, e.g., Dyson 1984).

On the other hand, the parameters of the ambient molecular cloud have been obtained from the integration of the ^{13}CO($J = 1 \rightarrow 0$) emission over the -41 to -38 km s^{-1} velocity range (central component, see § 2.3). We have used this molecule rather than C^{18}O because the higher signal-to-noise ratio of the ^{13}CO emission guarantee better quantitative values for the cloud parameters. We note that the ^{13}CO emission is also almost optically thin over the region ($\tau_{13} \leq 1$, see § 2.3). The total mass of $\geq 1240\ M_\odot$ we derived is consistent with the 1500 $M_\odot$ obtained by Arquilla & Goldsmith (1984). The velocity dispersion of the central component, $\sim$2–3 km s^{-1}, can be explained as motions gravitationally bound by the observed mass of the ambient cloud in a radius of $\sim 1'$ ($\sim 10^{-3}\ M_\odot$). The motions of the redshifted and blueshifted ^{13}CO com-

TABLE 3

OUTFLOW PARAMETERS[a]

Molecule (1)	V_{LSR} Range[b] (km s^{-1}) (2)	$\int T_R^* dV$ (K km s^{-1}) (3)	τ[c] (4)	N[d] (10^{16} cm^{-2}) (5)	$N(H_2)$[e] (10^{20} cm^{-2}) (6)	M[f] ($M_\odot$) (7)	$\dot{P}$[g] ($M_\odot$ km s^{-1} yr^{-1}) (8)	L_{mech}[h] ($L_\odot$) (9)
CO	(−55, −44)	22.2	0.5	1.6	1.6	∼0.3	$\sim 1 \times 10^{-4}$	∼0.1
^{13}CO	(−44, −41)	10.9	0.5	2.4	213	∼170	$\sim 4 \times 10^{-3}$	∼1.3
^{13}CO	(−38, −35)	8.7	0.3	1.7	151	∼80	$\sim 2 \times 10^{-3}$	∼0.6
CO	(−35, −24)	28.4	0.6	2.1	2.1	∼0.5	$\sim 1 \times 10^{-4}$	∼0.1

[a] Obtained from integration of the ^{13}CO($J = 1 \rightarrow 0$) emission over the inner wings, and integration of the CO($J = 2 \rightarrow 1$) emission over the outer wings (where ^{13}CO is not observable). Total mass, momentum rate, and mechanical luminosity of the outflow gas are the sum of the parameters given in cols. (7), (8), and (9), respectively.

[b] Velocity range used in the integration.

[c] Maximum value for the optical depth in the wings, obtained from the radiative transfer equation, assuming $T_{ex} = T_K = 30$ K (see § 2.3), and a filling factor of unity.

[d] CO and ^{13}CO column densities of the high-velocity gas, obtained from

$$N(\mathrm{CO}) = 3.2 \times 10^{14} \frac{\tau}{1 - e^{-\tau}} \frac{Q \int T_R^* dV \ (\mathrm{K\ km\ s^{-1}})}{[J(T_{ex}) - 0.19][1 - \exp(-11.06/T_{ex})]} \ \mathrm{cm^{-2}},$$

$$N(^{13}\mathrm{CO}) = 6.4 \times 10^{14} \frac{\tau}{1 - e^{-\tau}} \frac{Q \int T_R^* dV \ (\mathrm{K\ km\ s^{-1}})}{[J(T_{ex}) - 0.87][1 - \exp(-5.29/T_{ex})]} \ \mathrm{cm^{-2}},$$

where Q is the partition function, $J(T) = (h\nu/k)/[\exp(h\nu/kT) - 1]$, and $T_{ex} = T_K = 30$ K.

[e] Molecular hydrogen column density obtained from col. (5) and assuming abundances $[\mathrm{CO/H_2}] = 10^{-4}$ (Herbst & Leung 1989) and $[\mathrm{CO}/^{13}\mathrm{CO}] = 89$ (terrestrial ratio).

[f] Mass of the high-velocity gas obtained from col. (6) and from the FWHM of the integrated intensity maps of the wings.

[g] Momentum rate of the molecular outflow, MV^2/R, taking V as the largest observed relative velocity in each velocity range of integration, and $R \simeq 1$ pc as the size of the region with wing emission.

[h] Mechanical luminosity, $MV^3/2R$.

ponents, separated from the central component by ≤ 6 km s^{-1}, could also be gravitationally bound, tracing for example rotational motions. However, we favor that the ^{13}CO components are part of the molecular outflow since their bipolar distribution along the north–south direction is similar to that of the unbound (~ 15 km s^{-1}) CO outflow (see §§ 2.2 and 2.3).

TABLE 4

PARAMETER OF THE AMBIENT MOLECULAR CLOUD[a]

Parameter	Value
T_R (K)[b]	12.0
τ[c]	0.6
$\int T_R^* dV$ (K km s^{-1})[d]	25.1
N (10^{16} cm^{-2})[e]	6.1
$N(H_2)$ (10^{22} cm^{-2})[f]	5.4
$\theta_a \times \theta_b$ (arcsec)[g]	$\geq 140 \times 140$
M ($M_\odot$)[h]	≥1240
A_V (mag)[i]	54

[a] Obtained from the central component of the ^{13}CO($J = 1 \rightarrow 0$) spectrum (see § 2.5) at the position with the highest ^{13}CO integrated intensity.

[b] Maximum antenna temperature.

[c] Maximum optical depth, obtained from the radiative transfer equation assuming $T_{ex}(^{13}\mathrm{CO}) = T_K = 30$ K (see § 2.3), and a filling factor of unity.

[d] Integrated intensity over the range $-41 \leq V_{LSR} \leq -38$ km s^{-1}.

[e] ^{13}CO column density obtained from $N(^{13}\mathrm{CO}) = 6.4 \times 10^{14}[\tau/(1 - e^{-\tau})][Q \int T_R^* dV(\mathrm{K\ km\ s^{-1}})]/\{[J(T_{ex}) - 0.87][1 - \exp(-5.29/T_{ex})]\}$ cm^{-2}, where Q is the partition function, and $J(T) = (h\nu/k)/[\exp(h\nu/kT) - 1]$, with $T_{ex} = T_K = 30$ K.

[f] Molecular hydrogen column density obtained from $N(^{13}\mathrm{CO})$, assuming abundances $[\mathrm{CO}/^{13}\mathrm{CO}] \simeq 89$ (terrestrial ratio), and $[\mathrm{CO/H_2}] = 10^{-4}$ (Herbst & Leung 1989).

[g] FWHM of the ^{13}CO($J = 1 \rightarrow 0$) emission.

[h] Mass of the ambient cloud traced by the central component of the ^{13}CO($J = 1 \rightarrow 0$) emission obtained from f and g.

[i] Visual extinction, from $(A_V/\mathrm{mag}) \simeq 10 \times [N(H_2)/10^{22}$ cm$^{-2}]$ (Spitzer 1978).

From the ratio of the peak intensities of the ^{13}CO and C^{18}O lines, we estimate the relative abundance between these two molecules to be ~ 10, with no significant variation over the region. The H_2 column density of 5.4×10^{22} cm^{-2} given in Table 4 is consistent with the column density model presented by Arquilla & Goldsmith (1985) when extrapolated to areas within 1′ from the AFGL 437 cloud center (the size of our maps), and considering the different abundance adopted by these authors ($[^{13}\mathrm{CO/H_2} = 2 \times 10^{-6}]$) and the one we use ($[^{13}\mathrm{CO/H_2} = 1.1 \times 10^{-6}]$).

3. DISCUSSION

According to Wynn-Williams et al. (1981), the AFGL 437 cluster, which is also visible at optical wavelengths (Cohen & Kuhi 1977), is located close to the edge of the molecular cloud. We think the fact that this cluster may be breaking out of the cloud can lead to a reasonable explanation for the nature of the observed bipolar molecular outflow which is consistent with the previous work on the region.

In many star-forming regions with associated bipolar outflows, dense molecular gas structures are found to be aligned perpendicular to the outflow axis, and have been interpreted as responsible for the collimation of these outflows (see Rodríguez 1989 for a review). However, in AFGL 437, the central component of our ^{13}CO and C^{18}O data, which traces the ambient cloud, does not show any elongated structure that could be interpreted as an interstellar disk or toroid which collimates the outflow. A similar result was already reported in this region by Heyer et al. (1986) from CS observations.

Our high angular resolution and high-sensitivity observations give two important clues: (1) the very poor degree of collimation of the bipolar molecular outflow. It is hard to

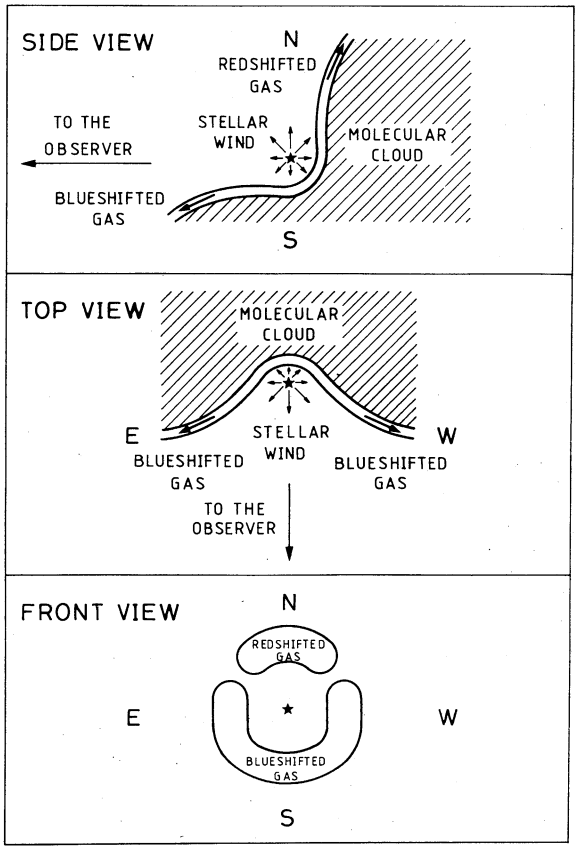

FIG. 7.—Proposed geometry for the outflow in AFGL 437

image how a disk or toroid can produce a blueshifted and redshifted component which is extended predominantly in the east–west direction (see § 2.2, and Figs. 3, 6*a*, and 6*c*). (2) The AFGL 437 cluster is not located at the center of the molecular outflow (see § 2.2), as it is usually observed in other outflow sources with elongated dense ambient molecular gas structures. We think that these two points indicate that the morphology of the molecular outflow in AFGL 437 is produced by other causes not related with disks or toroids around the powering source(s).

The peculiar characteristics found in the AFGL 437 molecular outflow lead us to suggest a geometrical model for the region, sketched in Figure 7. The young stars of the cluster, located at the edge of the molecular cloud (see also Fig. 3 of Wynn-Williams et al. 1981), can be undergoing mass loss through high-velocity winds (Wynn-Williams et al. 1981; Torrelles et al. 1992). In the past, these winds might have been able to open a cavity or hollow at the edge of the molecular cloud, sweeping clear and dispersing the molecular gas away from the cloud, making the AFGL 437 cluster visible at optical wavelengths. If the winds, which can be isotropic at the origin, shock obliquely against the walls of the hollow, they can produce, by a dragging effect, a laminar flow of molecular gas along the walls of the cavity according to the model of Calvet, Cantó, & Rodríguez (1981) and Cantó (1985) (see Fig. 7). This dragging of molecular gas, when observed under a particular angle of view, may give the appearance of a bipolar molecular outflow, with the red lobe to the north of the cluster and the blue lobe to the south. In this scenario—see Figure 7—blueshifted gas is expected to be also found at both sides of the cluster, as is better seen in ^{13}CO (Fig. 6*d*). Thus the apparent bipolarity could be caused by projection effects. The geometrical model we propose could explain the morphology of the lobes of the molecular outflow since these lobes would be delineating the walls of the cavity or hollow in the cloud. The inclination of the cavity relative to the line of sight would cause the IR cluster to appear projected on the red lobe of the outflow, according to our observations.

In summary, the main idea in our qualitative model is that the location of the AFGL 437 cluster at the edge of the molecular cloud, results in an asymmetric distribution of the ambient gas around the cluster. This leads to an apparent bipolar geometry for the outflow, which does not require any collimating mechanism such as disks or toroids. We note that the proposed geometric model can only explain qualitative results, and it cannot be used to predict detailed contour maps of the region.

4. CONCLUSIONS

We have observed the AFGL 437 region using the rotational transition lines of CO($J = 2 \rightarrow 1$), ^{13}CO($J = 1 \rightarrow 0$), and C^{18}O($J = 1 \rightarrow 0$). We also present water maser observations (6_{16}–5_{23}) toward this region. Our main conclusions can be summarized as follows.

1. The CO data show a high-velocity molecular outflow of complex morphology with a north–south bipolarity. However, in contrast with most outflows, the lobes of the molecular outflow are not elongated in the direction of the outflow axis, but in the perpendicular direction. This result indicates a very low degree of collimation.

2. The ^{13}CO spectra display three main velocity components, one of them coinciding with the velocity of the ambient cloud. The ^{13}CO blue and redshifted components show also a bipolar distribution along the north–south direction, similar to the CO high-velocity outflow. This bipolar morphology is also present in the C^{18}O lines.

3. We propose that the winds of the stars in the cluster might have been able to open a cavity or hollow at the edge of the molecular cloud. These winds can produce, by a dragging effect, a flow of molecular gas along the walls of the cavity. The position of the AFGL 437 cluster at the edge of the cloud may lead, through projection effects, to the appearance of a bipolar geometry for the molecular outflow.

4. We have detected two H_2O maser velocity components. We have measured their position and found that these components come from the center of the AFGL 437 cluster.

G. A., R. E., J. F. G., J. M. T., and L. V. acknowledge partial financial support from SEUI (Spain) grant PB87-0371. G. A. acknowledges support from Direcció General d'Universitats and CIRIT de Catalunya (Spain). J. F. G., J. M. T., and L. V. also acknowledge partial financial support from Junta de Andalucía (Spain). J. F. G. acknowledges support from a Smithsonian predoctoral fellowship.

REFERENCES

Arquilla, R., & Goldsmith, P. F. 1984, ApJ, 279, 664
———. 1985, ApJ, 297, 436
Calvet, N., Cantó, J., Rodríguez, L. F. 1981, BAAS, 13, 79
Cantó, J. 1985, in Cosmical Gas Dynamics, ed. F. D. Kahn (Manchester: VNU Science Press), 267
Cohen, M., & Kuhi, L. V. 1977, PASP, 89, 829
Dyson, J. E. 1984, Ap&SS, 106, 181
Gyulbudaghian, A. L., Rodríguez, L. F., & Mendoza-Torres, E. 1987, Rev. Mexicana Astron. Astrof., 15, 53
Herbst, E., & Leung, C. M. 1989, ApJS, 69, 271
Heyer, M. H., Snell, R. L., Goldsmith, P. F., Strom, S. E., & Strom, K. M. 1986, ApJ, 308, 134
Kleinmann, S. G., Sargent, D. G., Gillet, F. C., Grasdalen, G. L., & Joyce, R. R. 1977, ApJ, 215, L79
Kutner, M. L., & Ulich, B. L. 1981, ApJ, 250, 341
Lada, C. J. 1985, ARA&A, 23, 267
Parmar, P. S., Lester, D. F., Joy, M., Harvey, P. M., & Ellis, Jr, H. B. 1987, BAAS, 19, 728
Rainer, J., & McLean, I. 1987, in Infrared Astronomy with Arrays, ed. C. G. Wynn-Williams, E. E. Becklin, & L. H. Good (Honolulu: Univ. of Hawaii), 272
Rodríguez, L. F. 1989, in IAU Colloq. 120, Structure and Dynamics of the Interstellar Medium (New York: Springer), 197
Rodríguez, L. F., Carral, P., Ho, P. T. P., & Moran, J. M. 1982, ApJ, 260, 635
Schneps, M. H., Martin, R. N., Ho, P. T. P., & Barrett, A. H. 1978, ApJ, 221, 124
Spitzer, L. 1978, in Physical Process in the Interstellar Medium (New York: Wiley)
Torrelles, J. M., Gómez, J. F., Anglada, G., Estalella, R., Mauersberger, R., & Eiroa, C. 1992, ApJ, 392, 616
Wynn-Williams, C. G., Becklin, E. E., Beichman, C. A., Capps, R., & Shakeshaft, J. R. 1981, ApJ, 246, 801